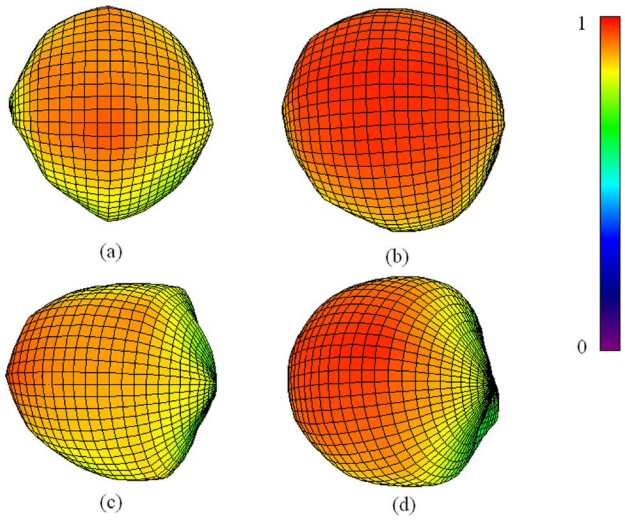

Fig. 6. The normalized full spherical radiation patterns of the slot antenna at different frequencies and working modes: (a) 0.8 GHz and (b) 1.48 GHz at the standard slot mode, (c) 0.42 GHz and (d) 0.96 GHz at the half-slot mode.

0.42 GHz to 1.48 GHz, achieving an extremely large frequency ratio of 3.52:1. In the small overlapped frequency range, antenna working in the half slot mode gives a better performance. Compared to the structure in [4], significantly fewer PIN diodes are used in the present antenna and our tuning range is much wider.

The full spherical radiation patterns of the antenna prototype were measured in a Lenovo Anechoic Chamber. In each operating mode, patterns at two frequencies (the highest and the lowest frequencies of that mode) were measured. The radiation patterns with a top view are presented in Fig. 6. One can see that the antenna gives consistent patterns within the whole tuning range. The measured gain is above -0.4 dB over the operating band.

IV. Conclusion

We have proposed in this letter a compact slot antenna that can be continuously tuned over a very wide frequency band. With only two lumped elements (a PIN diode and a varactor diode), a wide tuning range from 0.42 GHz to 1.48 GHz (with the frequency ratio of 3.52:1) has been achieved. Both the radiator and the feeding structure are quite simple. Good agreements between the simulated and measured results have been achieved in both modes. The measured full spherical radiation patterns are very consistent over the whole tuning range, and the measured gain is above -0.4 dB. This tunable antenna can be applied to radar or L-band communications and make the terminal devices compact.

Acknowledgment

The authors would like to thank Lenovo Company in Shanghai, China, for providing the full spherical radiation measurement.

References

[1] K. L. Wong, "Planar antennas for wireless communications," Microw. Opt. Eng. ser. Wiley Series in Microwave and Optical Engineering, pp. 26–69, 2003, ch. Ch.2.

[2] P. K. Panayi, M. O. Al-Nuaimo, and L. P. Ivrissimtzis, "Tuning techniques for planar inverted-F antenna," *Electron. Lett.*, vol. 37, no. 16, pp. 1003–1004, 2001.

[3] L. M. Feldner, C. T. Rodenbeck, C. G. Christodoulou, and N. Kinizie, "Electrically small frequency-agile PIFA-as-a-package for portable wireless devices," *IEEE Trans. Antennas Propag.*, vol. 55, no. 11, pp. 3310–3319, Nov. 2007.

[4] S. S. Yang, A. A. Kishk, and K. F. Lee, "Frequency reconfigurable U-slot microstrip patch antenna," *IEEE Antennas Wireless Propag. Lett.*, vol. 7, pp. 127–129, 2008.

[5] A. F. Sheta and S. F. Mahmoud, "A widely tunable compact patch antenna," *IEEE Antennas Wireless Propag. Lett.*, vol. 7, pp. 40–42, 2008.

[6] J. C. Ding;, Z. L. Lin;, Z. N. Ying, and S. L. He, "A compact ultra-wideband slot antenna with multiple notch frequency bands," *Microw. Opt. Tech. Lett.*, vol. 49, no. 12, pp. 3056–3060, 2007.

[7] D. Peroulis, K. Sarabandi, and L. P. B. Katehi, "Design of reconfigurable slot antennas," *IEEE Trans. Antennas Propag.*, vol. 53, no. 2, pp. 645–654, Feb. 2005.

[8] N. Behdad and K. Sarabandi, "Dual-band reconfigurable antenna with a very wide tenability range," *IEEE Trans. Antennas Propag.*, vol. 54, no. 2, pp. 409–416, Feb. 2006.

[9] C. R. White and G. M. Rebeiz, "Single- and dual-polarized tunable slot-ring antennas," *IEEE Trans. Antennas Propag.*, vol. 57, no. 1, pp. 19–26, Jan. 2009.

[10] M. I. Lai, T. Y. Wu, J. C. Hsieh, C. H. Wang, and S. K. Jeng, "Design of reconfigurable antennas based on an L-shaped slot and PIN diodes for compact wireless devices," *IET Microw. Antennas Propag.*, vol. 3, no. 1, pp. 47–54, 2009.

[11] R. Garg, P. Bhartia, I. Bahl, and A. Ittipiboon, *Microstrip Antenna Design Handbook*. Boston, London: Artech House, 2001, ch. Ch7.

[12] C. Y. Chiu, J. B. Yan, and R. D. Murch, "Compact three-port orthogonally polarized MIMO antennas," *IEEE Antennas Wireless Propag. Lett.*, vol. 6, pp. 619–622, 2007.

A Novel Compact UHF RFID Tag Antenna Designed With Series Connected Open Complementary Split Ring Resonator (OCSRR) Particles

Benjamin D. Braaten

***Abstract*—A novel compact planar antenna for passive UHF radio frequency identification (RFID) tags is presented. Instead of using meander-line sections, much smaller open complementary split ring resonator (OCSRR) particles are connected in series to create a small dipole with a conjugate match to the power harvesting circuit on the passive RFID tag. The manufactured (prototype) OCSRR RFID tag presented here has an antenna input impedance of $15.8 + j142.5\ \Omega$ at a frequency of 920 MHz and a max read range of 5.48 m. This performance is achieved with overall tag dimensions of $0.036\lambda_0 \times 0.17\lambda_0$ where λ_0 is the free space wavelength of 920 MHz.**

***Index Terms*—Dipole and passive tag, meander-line, open complementary split ring resonators, radio frequency identification (RFID).**

I. Introduction

The antenna is a major component in the layout of passive UHF radio frequency identification (RFID) tags. Previously, the meander-line antenna has been a popular design for compact passive UHF RFID tags [1]–[6]. A meander-line antenna is designed by bending the arms of a

Manuscript received August 31, 2009; revised November 30, 2009; accepted April 17, 2010. Date of publication August 30, 2010; date of current version November 03, 2010.

The author is with North Dakota State University, Electrical and Computer Engineering, Fargo, ND 58105 USA (e-mail: benbraaten@ieee.org).

Color versions of one or more of the figures in this communication are available online at http://ieeexplore.ieee.org.

Digital Object Identifier 10.1109/TAP.2010.2071348

printed dipole at right angles to create an electrically larger antenna in a smaller area [7]. The resulting antenna is a dipole with square-shaped sections along each dipole arm (Fig. 1(a)). The current on each vertical section (i.e., y-directed trace) of the dipole is in the opposite direction of the current on each adjacent vertical section. This results in a canceled far-field, thus the radiation of the meander-line antenna is mainly due to the horizontal sections. The behavior of the meander-line antenna in Fig. 1(a) can be described from a parallel circuit point-of-view. An equivalent capacitance exists between the longer parallel vertical traces, while the horizontal traces form an equivalent inductance. This results in a parallel LC-circuit representation of each meander-line section [8]. Thus, each meander-line pole can be thought of as several series connected parallel LC-circuits. Therefore, to achieve an inductive input impedance, the inductive part of each meander-line section needs to be dominant. This is especially important for electrically small antennas, because the input impedance can be capacitive [9], [10].

There are two major advantages of using a meander-line antenna. First, an inductive input impedance can be achieved with overall dimensions that are a fraction of the source wavelength. Second, the meander-line antenna only requires a single conducting layer. These two characteristics of a RFID antenna are very useful because it is usually desirable to have a small RFID tag printed on a single substrate (i.e., adhesive materials) with a conjugate match to the passive RFID integrated circuit (IC). Even though the meander-line antenna has resulted in small printed antenna designs, a smaller antenna is still very desirable. This is because a smaller RFID antenna can be used in many more applications and can be less costly to manufacture (less material).

Recently, a novel band pass filter (BPF) using an open complementary split ring resonator (OCSRR) particle was presented in [11]. This OCSRR BPF was implemented in coplanar waveguide (CPW) technology. The OCSRR particle is shown in Fig. 1(b) with the equivalent circuit shown in Fig. 1(c). The equivalent circuit of the OCSRR particle has the same equivalent circuit as each meander-line section in Fig. 1(a). Thus, series connected OCSRR particles have the same equivalent circuit as the series connected meander-line sections.

The work in this communication presents the application of using these OCSRRs in a manner similar to the series connected meander-line sections in Fig. 1(a). In particular, the particles of OCSRRs in Fig. 1(b) are connected in series to form the printed dipole shown in Fig. 2. The newly proposed design shown in Fig. 2 performs well as a RFID tag antenna and has the following very useful characteristics: 1) very simple to design; 2) very easy to manufacture; 3) only one conducting layer is required for normal operation thus avoiding complicated structures to enhance the performance; 4) each OCSRR particle is much smaller than the meander-line sections in previously published designs; 5) this antenna has a gain that is larger than other published meander-line antennas; and finally 6) the design presented in this communication is up to 50% smaller than commercially available tags with comparable read ranges [5].

II. The UHF RFID Tag Antenna With Series Connected OCSRR Particles

Other than the equivalent circuit in Fig. 1(c), the OCSRR presented in [11] was chosen for the design in Fig. 2 for two major reasons. First, each particle can be printed on a single conducting plane. This is very useful because, as mentioned before, antenna designs for passive UHF RFID tags are usually printed on a single adhesive dielectric substrate. For example, the design presented in this communication is much less complex than the metamaterial-based designs presented in [12]–[19]. Even though the antenna designs presented in [12]–[19] have promising results, the designs require complex ground structures, lumped elements and different materials to perform well. Using these techniques could result in a costly and complicated RFID tag. Second,

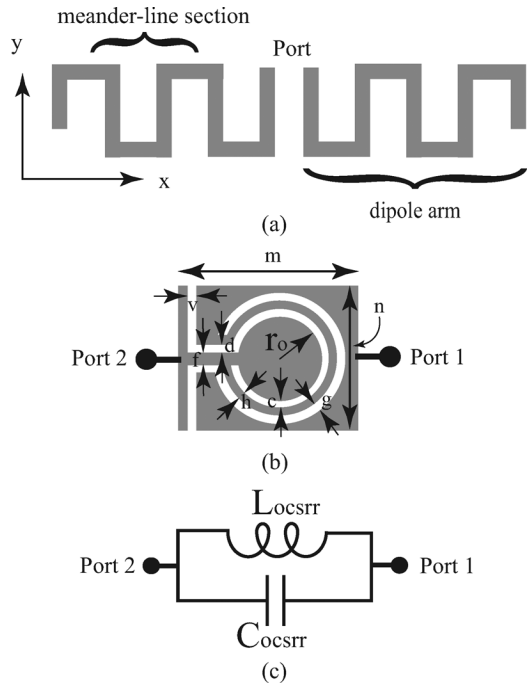

Fig. 1. (a) A meander-line antenna [8]; (b) the OCSRR particle (the gray area is the conducting plane); (c) the equivalent circuit of the OCSRR particle.

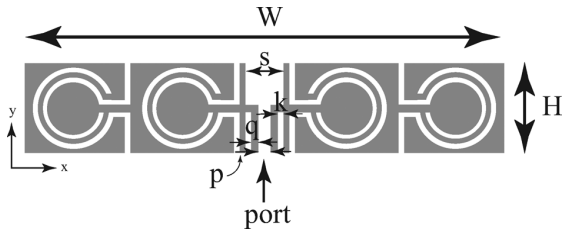

Fig. 2. The proposed UHF RFID antenna using series connected OCSRR particles.

the inductance of the OCSRR particle is four times than that of the complementary split ring resonator (CSRR) [11]. This makes the OCSRR particularly useful for compact UHF RFID antennas because the input impedance of an electrically small antenna is capacitive. By using several of the OCSRR particles connected in series, the input impedance of an electrically small antenna could be made inductive, which will be a conjugate match to the input impedance of the power harvesting circuit in the passive IC on the RFID tag.

The inductance of each particle is created by the loop of conducting material that has a width of h in Fig. 1(b) (i.e., the conducting loop between the two inner and outer ring slots). This conducting loop creates an electrical short between ports A and B. The capacitance in the particle is between the inner conducting disk with radius r_o and the surrounding outer conducting planes. These two structural features in the particle result in an equivalent inductance and capacitance connected in parallel. This resulted in the equivalent circuit in Fig. 1(c) [11]. By connecting the OCSRR particles in series and choosing a size of each particle were the inductance is dominant; a designer is able to produce a layout that resembles a thick printed dipole with periodic ring slots along the length of the dipole[1]. Having the layout resembling a thick printed dipole has the added advantage of increasing the input resistance and bandwidth [10]. This is very useful for matching the real part

[1]Further discussion on extracting the equivalent circuit of the OCSRRs can be found in [20].

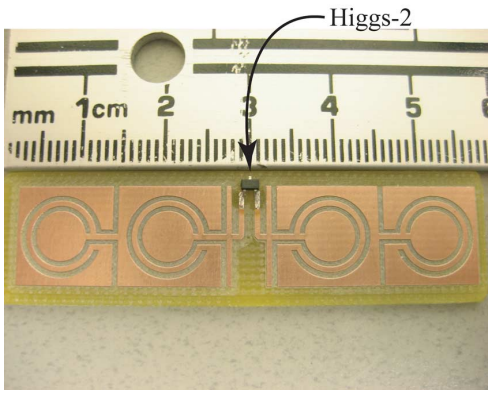

Fig. 3. The printed OCSRR RFID antenna on the prototype passive RFID tag ($c = 0.59$ mm, $d = 0.55$ mm, $f = 0.66$ mm, $g = 0.63$ mm, $h = 0.65$ mm, $k = 0.77$ mm, $m = 13.37$ mm, $n = 11.91$ mm, $p = 1.23$ mm, $q = 0.61$ mm, $r_o = 3.0$ mm, $s = 4.11$ mm, $W = 55.54$ mm, $H = 11.91$ mm and $v = 0.7$ mm).

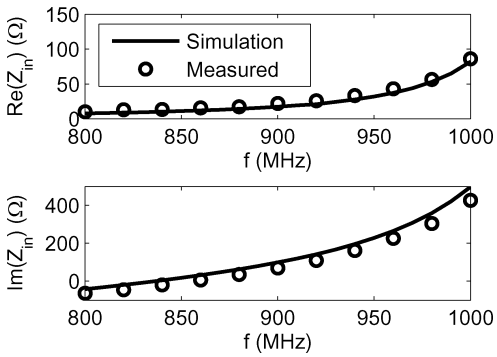

Fig. 4. Measured and simulated input impedance of the printed OCSRR antenna.

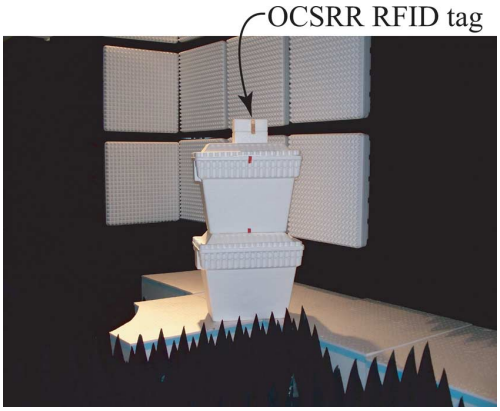

Fig. 5. Measuring the max read range of the prototype OCSRR RFID tag in Fig. 3.

of the input impedance of the antenna to the power harvesting circuit, especially because the input resistance of an electrically small antenna is very low.

A. Experimental Results and Validation

The first step was to design, manufacture and test a prototype passive RFID tag with the antenna in Fig. 2. Momentum [21] was used to design the printed antenna on 1.36 mm of FR-4 ($\varepsilon = 3.7$ measured and $\tan\delta = .011$ measured). The passive IC on the prototype RFID tag chosen was the Higgs-2 by Alien Technologies [22]. For a center frequency of 920 MHz, the Higgs-2 IC[2] has an input impedance of approximately $Z_{IC} = 13.73 - \mathrm{j}142.8\ \Omega$ [22]. Thus, the printed antenna design should be close to the conjugate of Z_{IC} at 920 MHz. This conjugate match requirement resulted in the printed design shown in Fig. 3. The size of each particle was determined experimentally in Momentum. The simulated and measured[3] input impedance results agreed well and are shown in Fig. 4. It should also be mentioned that the antenna presented in this communication has a 10 dB BW of 13 MHz.

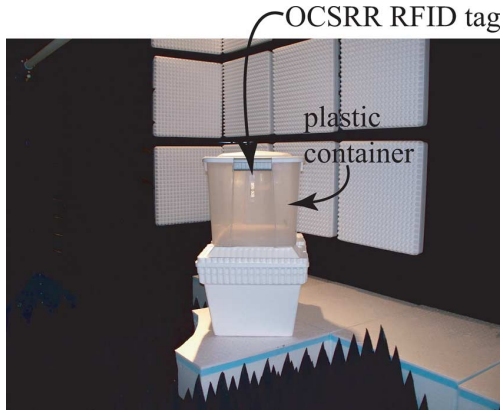

Fig. 6. Measuring the max read range of the prototype OCSRR RFID tag in Fig. 3 on a plastic container.

The next step was to determine how well the prototype RFID tag in Fig. 3 performed. The max read range of the tag was determined by attaching the tag to a piece of styrofoam. Then an Alien 9780 reader [22] (with a maximum output power of 1 W) connected to a CP antenna with a gain of 6 dBi and the prototype tag on the styrofoam were placed in an anechoic chamber. The experimental test is shown in Fig. 5. The prototype tag was moved away from the reader antenna and a max read range of 5.48 m was determined. Then, the prototype tag was placed on a plastic container (Fig. 6). This last test was performed to illustrate the performance of the prototype tag on a manufactured item. The max read range was then determined to be 5.33 m.

The good results in Fig. 4 and the large read range values of the prototype tag indicate that Momentum is an excellent and precise tool for modeling the antenna in Fig. 2. Therefore, because of the numerous designs in the next sections, Momentum will be used solely to calculate the input impedance and gain of a variety of printed OCSRR antennas. In particular, Momentum will be used to calculate the input impedance and gain of the OCSRR antenna in Fig. 3 on various substrate permittivities ε, substrate thicknesses d and with several values of r_o (i.e., disk radius values). These results will then be followed with Figures showing the surface current on the OCSRR antenna and the far-field patterns. Investigating these problems extensively will demonstrate the behavior of the OCSRR antenna presented in this communication. This could be very useful for a designer because a short review of the following sections may determine if the OCSRR antenna presented in this communication is suited for a particular application of a passive UHF RFID tag.

[2]The sensitivity during a read is -14 dBm and the sensitivity during programming is -10 dBm. Also, the equivalent input impedance is a 1.5 KΩ resistor connected in parallel with a 1.2 pF capacitor [22].

[3]To measure the input impedance, the printed antenna was cut symmetrically down the middle, placed vertically above a ground plane and fed with an SMA connector through the ground plane. The input impedance of the monopole was then measured using a calibrated network analyzer. The measured value was then multiplied by two to correspond to the dipole simulations in Momentum.

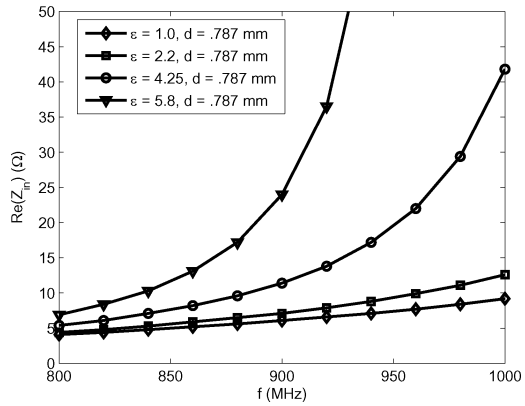

Fig. 7. Input resistance for various values of ε.

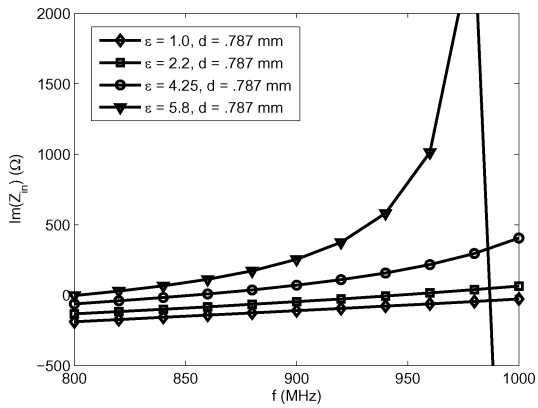

Fig. 8. Input reactance for various values of ε.

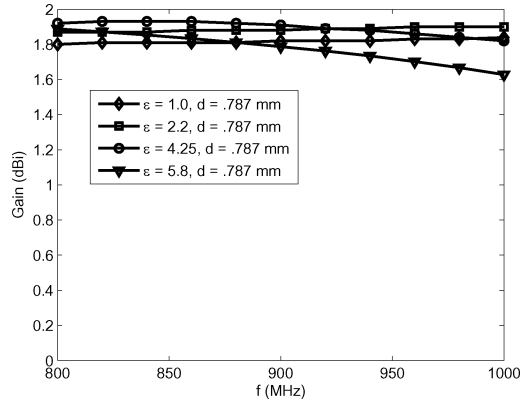

Fig. 9. Gain for various values of ε.

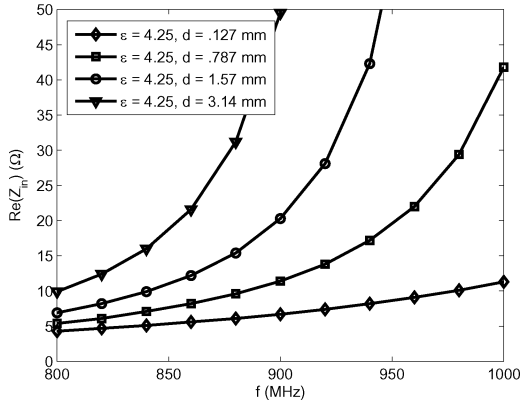

Fig. 10. Input resistance for various values of d.

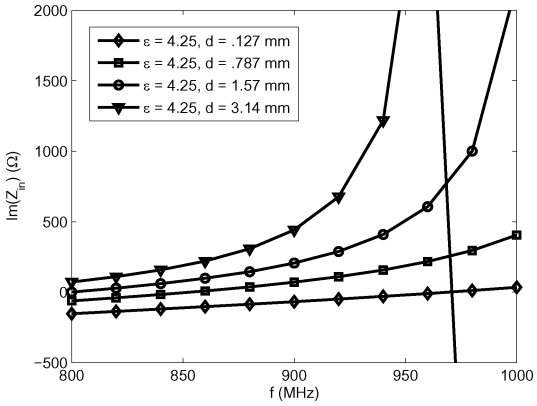

Fig. 11. Input reactance for various values of d.

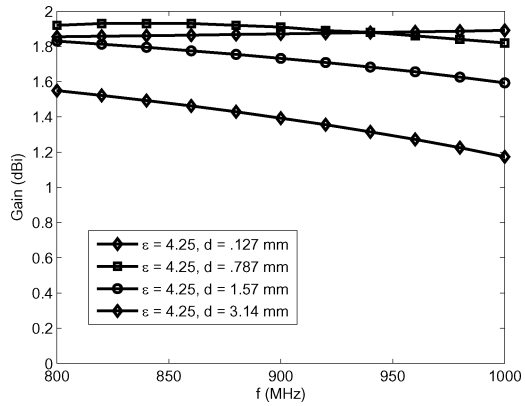

Fig. 12. Gain for various values of d.

B. Results for Various Values of Permittivity

First, the permittivity ε of the substrate was varied and d was set at 0.787 mm. This illustrated how the input impedance and gain were affected by different values of ε. The results from these simulations are shown in Figs. 7 – 9. The results in Fig. 7 show the rate at which the input resistance increases for larger values of ε while Fig. 8 shows how the antenna becomes more inductive for larger values of ε. The results in Fig. 9 show a max gain of 1.89 dBi at 920 MHz and that the gain reduces slightly for larger values of ε.

C. Results for Various Values of Substrate Thickness

Second, the thickness d of the substrate was changed and ε was set at 4.25. This illustrated how the input impedance and gain were affected by different values of d. The results from these simulations are shown in Figs. 10 – 12. The results in Fig. 10 show how the input resistance can increase substantially for larger values of d and Fig. 11 shows that the antenna becomes more inductive (i.e., resonates at a lower frequency) for larger values of d. The results in Fig. 12 show a max gain of 1.89 dBi at 920 MHz and that the gain can be significantly reduced for larger values of d.

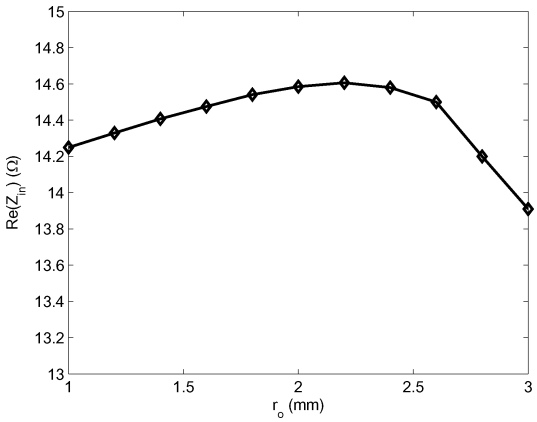

Fig. 13. Input resistance for various values of r_o with $\varepsilon = 4.25$ and $\mathrm{d} = 0.787$ mm.

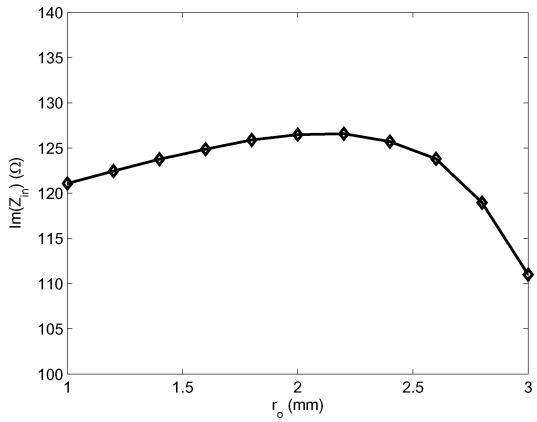

Fig. 14. Input reactance for various values of r_o with $\varepsilon = 4.25$ and $\mathrm{d} = 0.787$ mm.

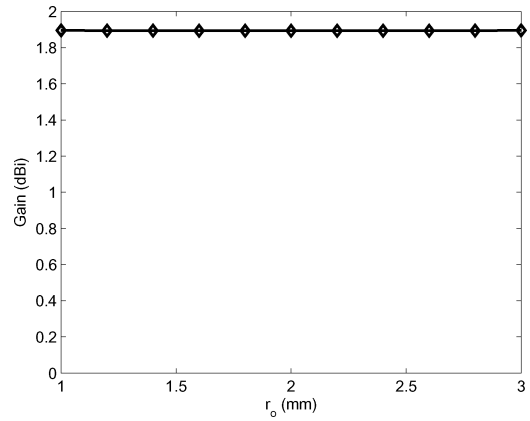

Fig. 15. Gain for various values of r_o with $\varepsilon = 4.25$ and $\mathrm{d} = 0.787$ mm.

D. Results for Various Values of Inner Disk Radius

Next, the radius of the inner disk r_o was varied and the source frequency was set to 920 MHz. This illustrated how the input impedance and gain were affected by different values of r_o. The results from these simulations are shown in Figs. 13 – 15. The results in Fig. 13 show that the input resistance varies less than an ohm for various values of r_o, while Fig. 14 shows that the input reactance of the antenna only varies by a few ohms for r_o approximately less than 2.6 mm. Then, the capacitance between the inner disk and outer conducting plane becomes more significant for $r_o \geq 2.6$ mm. After this value, the input reactance begins to reduce much more rapidly. The results in Fig. 15 show a max gain of 1.89 dBi and that the gain is mostly unaffected by the radius of the inner disk.

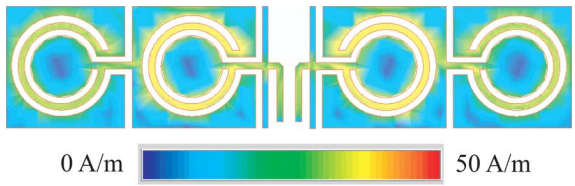

Fig. 16. Surface currents on the printed OCSRR antenna in Fig. 3 with $\varepsilon = 3.7$ and $\mathrm{d} = 1.36$ mm..

E. Surface Currents and Far-Field Patterns

Finally, the surface currents and far-field patterns were determined at 920 MHz. The surface currents on the OCSRR antenna are shown in Fig. 16. Notice the currents concentrated on the inner conducting ring. The normalized dominant far-field patterns for the x-z and y-z planes are shown in Figs. 17 and 18, respectively. The far-field patterns are similar to the patterns of a small dipole.

III. Discussion

Many noteworthy comments can be made about the results in Figs. 3, 5 and 7 – 18.

1) The dimensions in Fig. 3 show that the OCSRR UHF RFID antenna presented in this communication is much smaller (55.54 mm × 11.91 mm or $0.036\lambda_0 \times 0.17\lambda_0$) than commercially available tags.
2) The measurements shown in Fig. 5 demonstrate that the prototype tag in Fig. 3 has a max read range (5.48 m) comparable to other published and commercially available passive RFID tags with twice the overall size.
3) In Figs. 7 and 10, it is shown how the input resistance can be controlled with values of ε and d, respectively.
4) In Figs. 8 and 11, it is shown how the antenna can be designed to operate at a lower frequency with larger values of ε and d, respectively. These results are similar to the metamaterial-based antennas presented in [4].
5) From the results in Figs. 9 and 12, it can be concluded that the gain of the antenna can be increased by using smaller values of ε and d, respectively.
6) The results in Figs. 13 and 14 show that the particle inductance can be used effectively to match the input reactance of the antenna with the reactance of the tag.
7) The patterns shown in Figs. 17 and 18 are similar to a small dipole.

IV. Conclusions

A new compact UHF RFID tag antenna designed using series connected OCSRR particles was presented. The series connected OCSRR particles were modeled in Momentum and the simulated input impedance values were successfully validated with measurements. The result was a compact UHF RFID tag with a read range of 5.48 m. This read range was accomplished with an overall antenna dimension up to 50% smaller than commercially available RFID tags with comparable read ranges. Next, the properties of the substrate and dimensions of the inner disk were varied. Each of these changes were modeled numerically in Momentum and the input impedance and gain was determined for the different substrate and inner disk values. These simulations were done to illustrate the behavior of

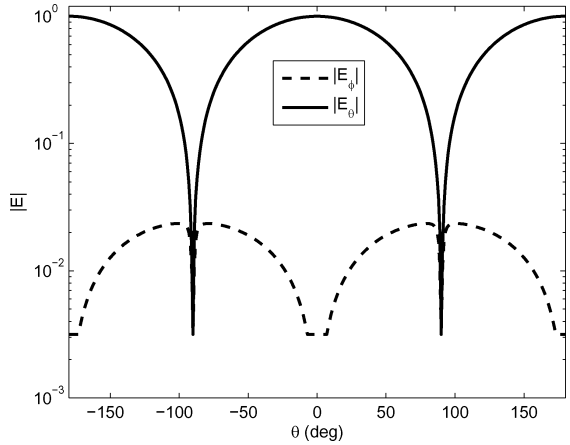

Fig. 17. Normalized pattern in the x-z plane of the printed OCSRR antenna in Fig. 3 with $\varepsilon = 3.7$ and $\mathrm{d} = 1.36\ \mathrm{mm}$.

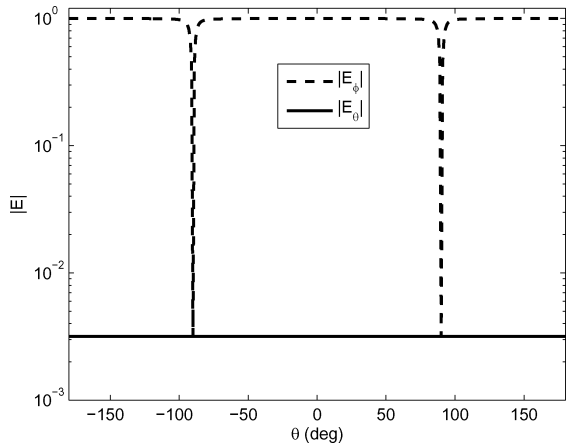

Fig. 18. Normalized pattern in the y-z plane of the printed OCSRR antenna in Fig. 3 with $\varepsilon = 3.7$ and $\mathrm{d} = 1.36\ \mathrm{mm}$..

the novel OCSRR RFID antenna presented in this communication. Finally, the surface currents and far-field patterns were determined. The OCSRR antenna presented in this communication has a pattern similar to a small dipole.

ACKNOWLEDGMENT

The authors would like to thank A. Reinholz and M. Reich, at the Center for Nanoscale Science and Engineering (CNSE), North Dakota State University, for supporting various aspects of this project.

REFERENCES

[1] K. Finkenzeller, *RFID Handbook: Fundamentals and Applications in Contactless Smart Cards and Identification*. West Sussex, U.K.: Wiley, 2003.

[2] G. Marrocco, "Gain-optimized self-resonant meander line antennas for RFID applications," *IEEE Antennas Wireless Propag. Lett.*, vol. 2, pp. 302–305, 2003.

[3] C. Calabrese and G. Marrocco, "Meander-slot antennas for sensor-RFID tags," *IEEE Antennas Wireless Propag. Lett.*, vol. 7, pp. 5–8, 2008.

[4] B. D. Braaten, R. P. Scheeler, M. Reich, R. M. Nelson, C. Bauer-Reich, J. Glower, and G. J. Owen, "Compact metamaterial-based UHF RFID antennas: Deformed omega and split-ring resonator structures," *ACES Special Issue on Comput. Experimental Tech. RFID Syst. Applicat.*, to be published.

[5] B. D. Braaten, M. Reich, and J. Glower, "A compact meander-line UHF RFID tag antenna loaded with elements found in right/left-handed coplanar waveguide structures," *IEEE Antennas Wireless Propag. Lett.*, vol. 8, pp. 1158–1161, 2009.

[6] B. D. Braaten, G. J. Owen, D. Vaselaar, R. M. Nelson, C. Bauer-Reich, J. Glower, B. Morlock, M. Reich, and A. Reinholz, "A Printed Rampart-line antenna with a dielectric superstrate for UHF RFID applications," presented at the IEEE Int. Conf. on RFID, Las Vegas, NV, Apr. 16–17, 2008.

[7] H. Nakano, H. Tagami, A. Yoshizawa, and J. Yamauchi, "Shortening ratios of modified dipole antenna," *IEEE Trans. Antennas Propag.*, vol. AP-32, no. 4, pp. 385–386, Apr. 1984.

[8] R. Bancroft, *Microstrip and Printed Antenna Design*. Raleigh, NC: Scitech Publishing, 2006, pp. 194–195.

[9] W. L. Stutzman and G. A. Thiele, *Antenna Theory and Design*, 2nd ed. New York: Wiley, 1998.

[10] C. A. Balanis, *Antenna Theory: Analysis and Design*, 3rd ed. New York: Wiley, 2005.

[11] A. Velez, F. Aznar, J. Bonache, M. C. Valazquez-Ahumada, J. Martel, and F. Martin, "Open complementary split ring resonators (OCSRRs) and their application to wideband CPW band pass filter," *IEEE Microw. Wireless Comp. Lett.*, vol. 19, no. 4, pp. 197–199, Apr. 2009.

[12] R. W. Ziolkowski and C.-C. Lin, "Metamaterial-inspired magnetic-based UHF and VHF antennas," in *IEEE Antennas Propag. Soc. Int. Symp. Dig.*, San Diego, CA, Jul. 5–11, 2008.

[13] C.-J. Lee, K. M. K. H. Leong, and T. Itoh, "Composite right/left-handed transmission line based compact resonant antennas for RF module integration," *IEEE Trans. on Antennas Propag.*, vol. 54, no. 8, pp. 2283–2291, Aug. 2006.

[14] Q. Liu, P. S. Hall, and A. L. Borja, "Dipole with left handed loading with optimised efficiency," in *Proc. EuCAP*, Edinburgh, U.K., Nov. 11–16, 2007, pp. 1–4.

[15] H. Iizuka and P. S. Hall, "Left-handed dipole antennas and their implementations," *IEEE Trans. Antennas Propag.*, vol. 55, no. 5, pp. 1246–1253, May 2007.

[16] M. A. Y. Abdalla, K. Phang, and G. V. Eleftheriades, "A planar electronically steerable patch array using tunable PRI/NRI phase shifters," *IEEE Trans. Microw. Theory Tech.*, vol. 57, no. 3, pp. 531–541, Mar. 2009.

[17] F. J. Herraz-Martinez, P. S. Hall, Q. Liu, and D. Segovia-Vargas, "Tunable left-handed monopole and loop antennas," presented at the IEEE Antennas Propag. Soc. Int. Symp. Dig., Charleston, SC, Jun. 1–5, 2009.

[18] J. Dacuna and R. Pous, "Miniaturized UHF tags based on metamaterials geometries," *Building Radio Frequency Identification for the Global Environment*, Jul. 2007.

[19] M. Stupf, R. Mittra, J. Yeo, and J. R. Mosig, "Some novel design for RFID antennas and their performance enhancement with metamaterials," *Microw. Optical Tech. Lett.*, vol. 49, no. 4, pp. 858–867, Feb. 2007.

[20] F. Aznar, A. Velez, M. Duran-Sindreu, J. Bonache, and F. Martin, "Elliptic-function CPW low-pass filters implemented by means of open complementary split ring resonators (OCSRRs)," *IEEE Microw. Wireless Comp. Lett.*, vol. 19, no. 11, pp. 689–6919, Nov. 2009.

[21] Advanced Design System-ADS Agilent Technologies, 2009.

[22] Alien Technologies [Online]. Available: www.alientechnologies.com